Supporting Information: The Onset of H + Ketene Products from Vinoxy Radicals Prepared by Photodissociation of Chloroacetaldehyde at 157 nm

Chow-Shing Lam, Jonathan D. Adams, and Laurie J. Butler*

**The James Franck Institute and Department of Chemistry, The University of Chicago, Chicago, Illinois 60637 USA*

Contents

A. Geometries of the Conformers of Chloroacetaldehyde

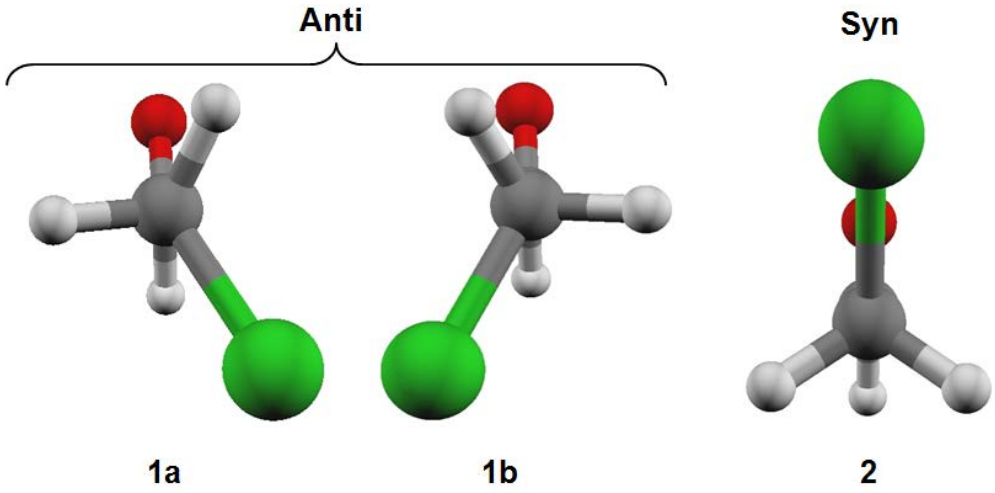

Figure S1. Geometries of the conformers of chloroacetaldehyde. The lower labels are used when it is necessary to denote a specific conformer.

Cartesian Coordinates (Å) for Conformer Geometries Calculated at B3LYP/6-311++G(3df,2p) level

1a;

C	-1.196270	-0.306673	0.220802
O	-2.299665	-0.071618	-0.185696
H	-0.942720	-1.262367	0.717052
C	-0.062965	0.692929	0.110119
H	-0.021112	1.291401	1.020339
H	-0.213692	1.342945	-0.746343
Cl	1.517936	-0.139332	-0.057184

1b;

C	1.196271	-0.306683	0.220786
O	2.299673	-0.071609	-0.185687
H	0.942723	-1.262397	0.717001
C	0.062970	0.692918	0.110119
H	0.021121	1.291378	1.020347
H	0.213694	1.342948	-0.746334
Cl	-1.517942	-0.139327	-0.057182

2;

C	1.394561	0.386988	0.000000
O	1.681330	-0.773687	0.000000

H	2.175794	1.177551	0.000000
C	0.000000	0.968627	0.000000
H	-0.111105	1.604722	0.879851
H	-0.111105	1.604722	-0.879851
Cl	-1.303913	-0.237744	0.000000

B. EOM-CCSD Calculations of the Excited States of Chloroacetaldehyde along the C-Cl Coordinate

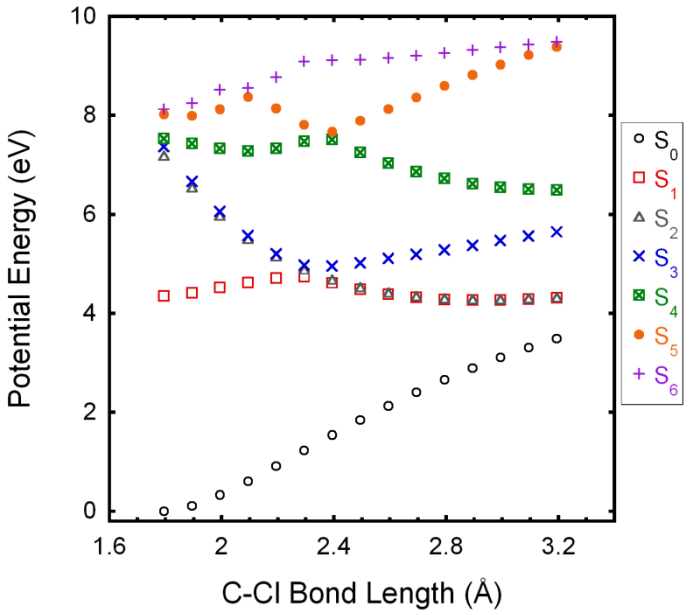

Figure S2. Singlet excited states of chloroacetaldehyde along the C-Cl coordinate calculated at the EOM-CCSD/6-311++G(3df,2p) level of theory. Geometries are optimized geometries on the ground state (S_0) at each C-Cl internuclear distance, so the asymptotes do not reach the minimum energy of the channel.

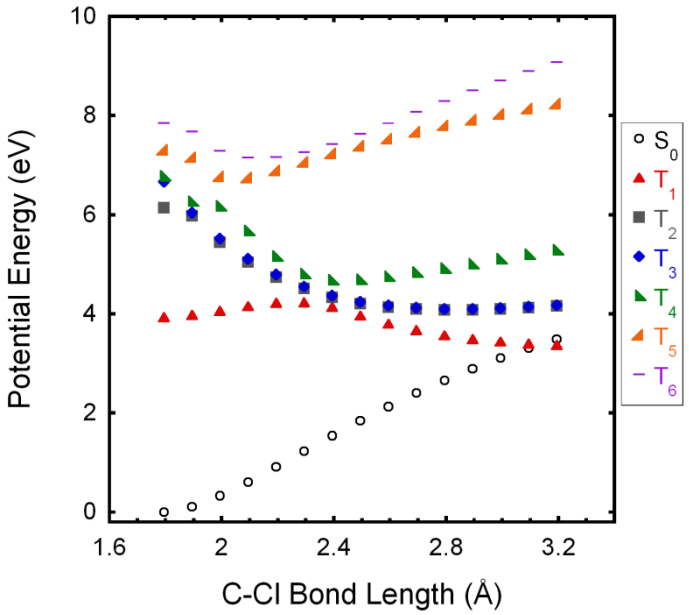

Figure S3. Triplet excited states of chloroacetaldehyde along the C-Cl coordinate calculated at the EOM-CCSD/6-311++G(3df,2p) level of theory. Geometries are the optimized geometries on the ground state (S_0) at each C-Cl internuclear distance, so the asymptotes do not reach the minimum energy of the channel.

We also performed the EOM-CCSD calculations with the smaller aug-cc-pVDZ basis set. While the points were slightly lower in energy, the overall shapes of the surfaces were still the same. Note that the EOM-CCSD method does not accurately treat the geometries at large C-Cl bond lengths, so we have used these preliminary calculations only to inform us of the shape of the potential energy surfaces in the Franck-Condon region and at intermediate C-Cl bond distances

C. Rough Division of the C-Cl Bond Fission $P(E_T)$ to Access the $Cl(^2P_{1/2})/Cl(^2P_{3/2})$ Branching Ratio in the Fast Component and the Portion of the Slow Component that Can Produce $\tilde{B}$ State Vinoxy

Here we present a rough division of the C-Cl bond fission $P(E_T)$ into a slow portion for which the $\tilde{B}$ state of vinoxy is energetically allowed (energies less than E_T = 20 kcal/mol), a fast portion peaking near 40 kcal/mol, and an intermediate portion. This division is somewhat arbitrary, so we show two options and the corresponding $Cl(^2P_{1/2})/Cl(^2P_{3/2})$ branching ratios for each. The first option attempts to capture the full features of the fast portion without making these portions similar for the $Cl(^2P_{1/2})$ and $Cl(^2P_{3/2})$ $P(E_T)$s. The second option constrains the fast portion to be similar in shape for both the $Cl(^2P_{1/2})$ and $Cl(^2P_{3/2})$ $P(E_T)$s.

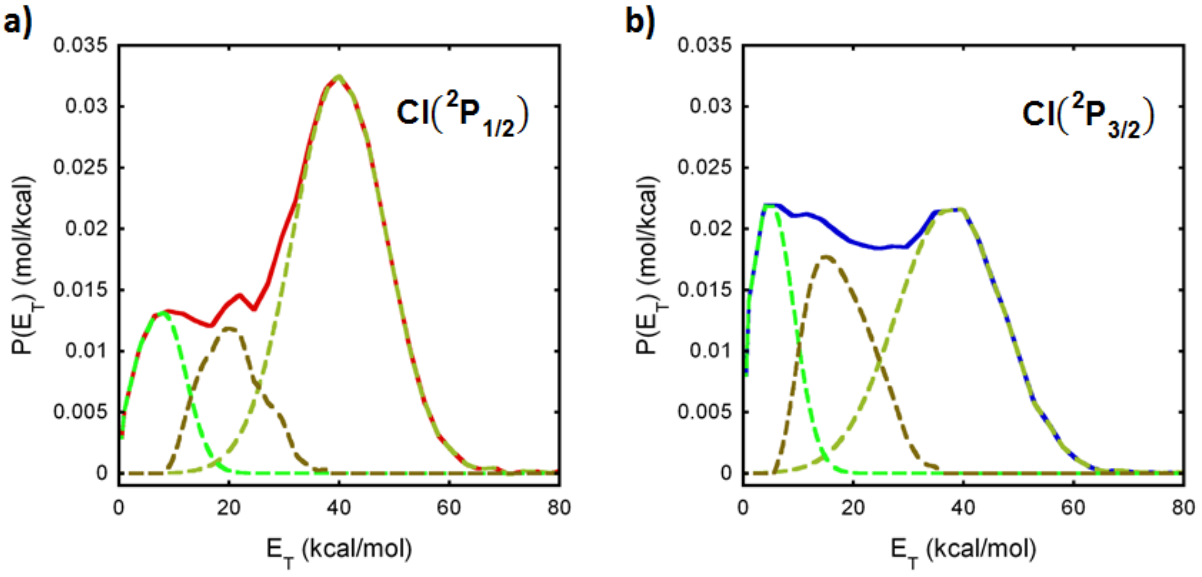

Figure S4. First option for dividing the C-Cl bond fission $P(E_T)$ into a slow portion that can produce $\tilde{B}$ state vinoxy, a fast portion that peaks near 40 kcal/mol, and an intermediate portion. Panel (a) shows the components of the C-Cl bond fission $P(E_T)$ for $Cl(^2P_{1/2})$ in dashed line in varying shades of green and the total $P(E_T)$ for this spin-orbit state shown in solid red line. Panel (b) shows the components of the C-Cl bond fission $P(E_T)$ for $Cl(^2P_{3/2})$ in dashed line with the same coloring scheme and the total $P(E_T)$ for this spin-orbit state in solid blue line.

Table S1. Ratios of the Signal Intensity between the $P(E_T)$s for each Spin Orbit State and $Cl(^2P_{1/2})/Cl(^2P_{3/2})$ Branching Ratios for Each Component of the C-Cl Bond Fission $P(E_T)$ following the First Option for the Division

Portion of $P(E_T)$	$S[Cl(^2P_{1/2})]/S[Cl(^2P_{3/2})]$	$Cl(^2P_{1/2})/Cl(^2P_{3/2})$ Branching Ratio
Fast	1.30	1.10
Slow	0.73	0.62
Intermediate	0.62	0.53

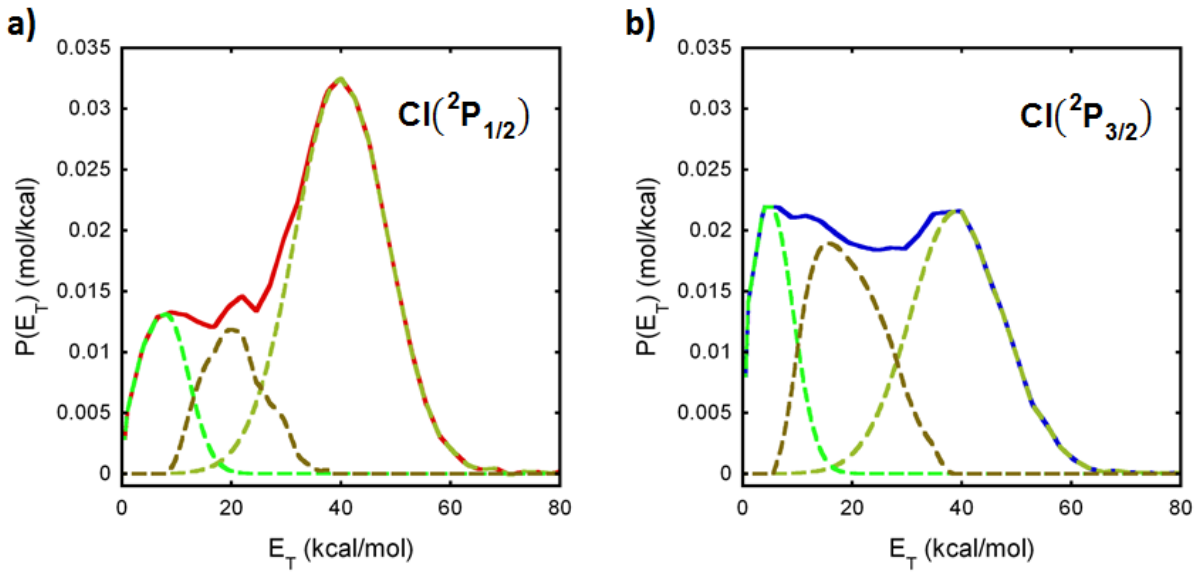

Figure S5. Second option for dividing the C-Cl bond fission $P(E_T)$ into a slow portion that can produce $\tilde{B}$ state vinoxy, a fast portion that peaks near 40 kcal/mol, and an intermediate portion. Panel (a) shows the components of the C-Cl bond fission $P(E_T)$ for $Cl(^2P_{1/2})$ in dashed line in varying shades of green and the total $P(E_T)$ for this spin-orbit state shown in solid red line. Panel (b) shows the components of the C-Cl bond fission $P(E_T)$ for $Cl(^2P_{3/2})$ in dashed line with the same coloring scheme and the total $P(E_T)$ for this spin-orbit state in solid blue line.

Table S2. Ratios of the Signal Intensity between the $P(E_T)$s for each Spin Orbit State and $Cl(^2P_{1/2})/Cl(^2P_{3/2})$ Branching Ratios for Each Component of the C-Cl Bond Fission $P(E_T)$ following the Second Option for the Division

Portion of $P(E_T)$	$S[Cl(^2P_{1/2})]/S[Cl(^2P_{3/2})]$	$Cl(^2P_{1/2})/Cl(^2P_{3/2})$ Branching Ratio
Fast	1.49	1.27
Slow	0.72	0.62
Intermediate	0.50	0.42

D. Speed Dependence of the Anisotropy Parameter $\beta_2(v)$ for $Cl(^2P_{3/2})$ and $Cl(^2P_{1/2})$

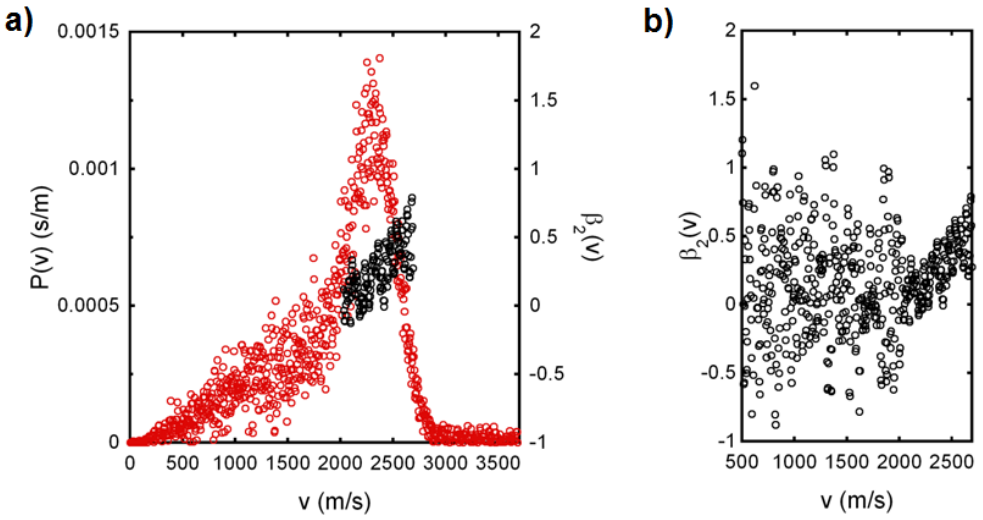

Figure S6. Speed dependence of the anisotropy parameter $\beta_2(v)$ for $Cl(^2P_{1/2})$. Panel (a) shows the anisotropy values (black circles) overlaid on the high kinetic energy portion of the $Cl(^2P_{1/2})$ speed distribution (red circles). Panel (b) shows how the anisotropy varies from near isotropic in the slow portion of the speed distribution to weakly parallel in the high kinetic energy portion.

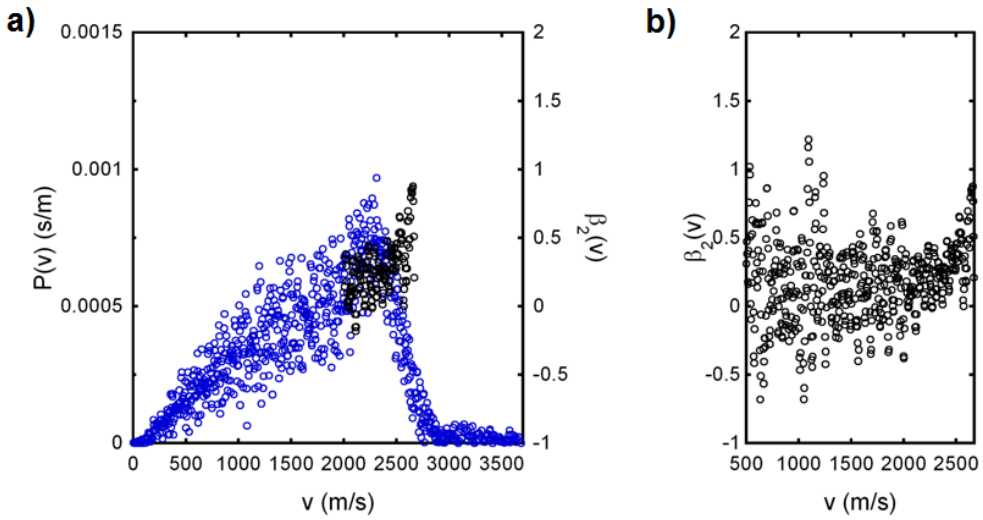

Figure S7. Speed dependence of the anisotropy parameter $\beta_2(v)$ for $Cl(^2P_{3/2})$. Panel (a) shows the anisotropy values (black circles) overlaid on the high kinetic energy portion of the $Cl(^2P_{3/2})$ speed distribution (red circles). Panel (b) shows how the anisotropy varies from near isotropic in the slow portion of the speed distribution to weakly parallel in the high kinetic energy portion.

E. Correction to the Effective Barrier Height Caused by the Shift of the Minimum or Saddle Point to a Nearby Geometry along the IRC

The effective barrier height we use for our branching calculations represents the energy difference between the minimum and the saddle point on the rotationally corrected IRC, which we get by adding rotational energy to our calculated IRC (which has $J_{rot} = 0$). These rotational corrections can actually cause the minimum and/or saddle point to shift to a different geometry along the IRC, usually nearby. In this case, we need to use the E_{rot}/E_T ratios at the new minimum geometry and/or new saddle point geometry. However, this is not the only correction we have to make. The new minimum and new saddle point geometries also have different potential energies and so we have to redefine the energetics (Figure S8).

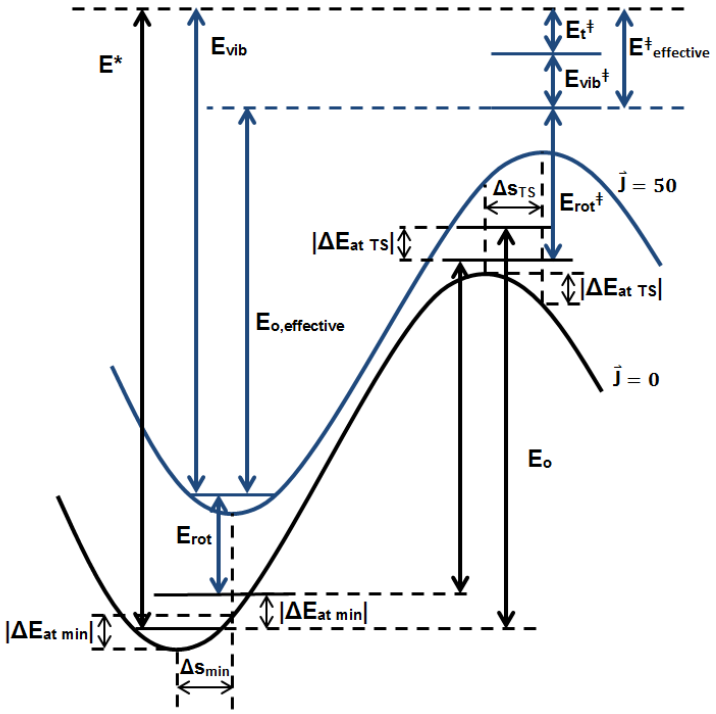

Figure S8. Diagram of the energetics involved in a unimolecular reaction in which the minimum and saddle point geometries of the rotationally corrected IRC differ from that of the IRC with $\vec{J}_{rot} = 0$ by Δs_{min} and Δs_{TS}. E* is the total internal energy in the radical which consists of vibrational energy, E_{vib}, and rotational energy, E_{rot}. $E^{\ddagger}$ is the total internal energy at the critical configuration which consists of vibrational energy, $E_{vib}^{\ddagger}$, rotational energy, $E_{rot}^{\ddagger}$, and the translational energy along the reaction coordinate, $E_t^{\ddagger}$. E_o is the energy difference between the zero-point energy of the radical and that of the critical configuration, thus representing the barrier height. Note how the potential energies of the new minimum and saddle point geometries differ from that of the IRC with $\vec{J}_{rot} = 0$ by $|\Delta E_{at\ min}|$ and $|\Delta E_{at\ TS}|$, respectively. The effective barrier height, $E_{o,\ effective}$, is now the energy difference between the energy of the new minimum geometry ($E_{rot} + |\Delta E_{at\ min}|$) and the energy of the new saddle point ($E_o + E_{rot}^{\ddagger} - |\Delta E_{at\ TS}|$).

We calculate these terms using the B3LYP energies from the IRC calculation. So, the full expression for calculating the effective barrier heights is given by

$$E_{o,\ effective} = E_0 + \left[\left(\frac{E_{rot}}{E_T}\right)_{at\ TS} - \left(\frac{E_{rot}}{E_T}\right)_{at\ min}\right] E_T - |\Delta E_{at\ TS}| - |\Delta E_{at\ min}|$$

The effective barrier is used in the RRKM calculations.

F. Description of the Permutation Vectors Used in our Rotational Model

Our rotational model transforms the geometry of the radical moiety into any stationary point geometry while preserving the magnitude and direction of the angular momentum vector. In order to accomplish the desired transformation, the model calls for a "permutation vector," which maps the atoms in the moiety configuration to their corresponding position in the stationary point configuration. The permutation vector basically tells the program how the atoms in the moiety are arranged in the stationary point. In most cases, determining how the atoms in the stationary point are related to the atoms in the moiety is trivial. This is especially true for atoms that make up the backbone structure of a molecule, like the C atoms and O atom in the chloroacetaldehyde moiety which have similar positions in all of the stationary points. Assigning the H atom in the aldehyde group is also trivial as it is easy to tell where it is in the stationary points. However, assigning the positions of terminal H atoms is often tricky as there are a few possibilities and they can have a big effect on the rotational energy in the stationary point (Figure S9).

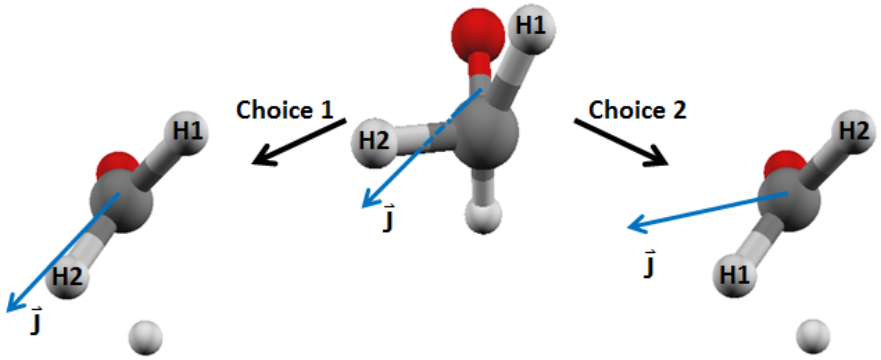

Figure S9. Depiction of the effects of the permutation vector on the rotational energy in the stationary point. The radical moiety of the anti conformer of chloroacetaldehyde is shown in the center looking along the C-C bond with the O atom is attached to the back carbon. There are two distinct possible choices for the permutation vector leading to the kTS1 transition state in which the H atoms in the moiety (attached to the front carbon and denoted "H1" and "H2") are going to different position in the kTS1 structure. Note how changing where the H atoms go in kTS1 changes the relative position of the angular momentum vector, $\vec{J}$, compared to geometry of the molecule. We say "relative to the geometry of the molecule" because $\vec{J}$ should not change its direction nor magnitude and so only the geometry of molecule with respect to $\vec{J}$ should change. This will result in different E_{rot}/E_T ratios and thus different rotational energies.

In choosing the permutation vector, we assumed that the correct permutation would minimize the displacement of the terminal H atoms in the moiety to get to the vinoxy radical. From there, the permutation vector leading to the transition states are dictated by the assignment of the H atoms in the vinoxy radical. The figures below show all of the permutations for the terminal H atoms that we used for each of the conformers of chloroacetaldehyde.

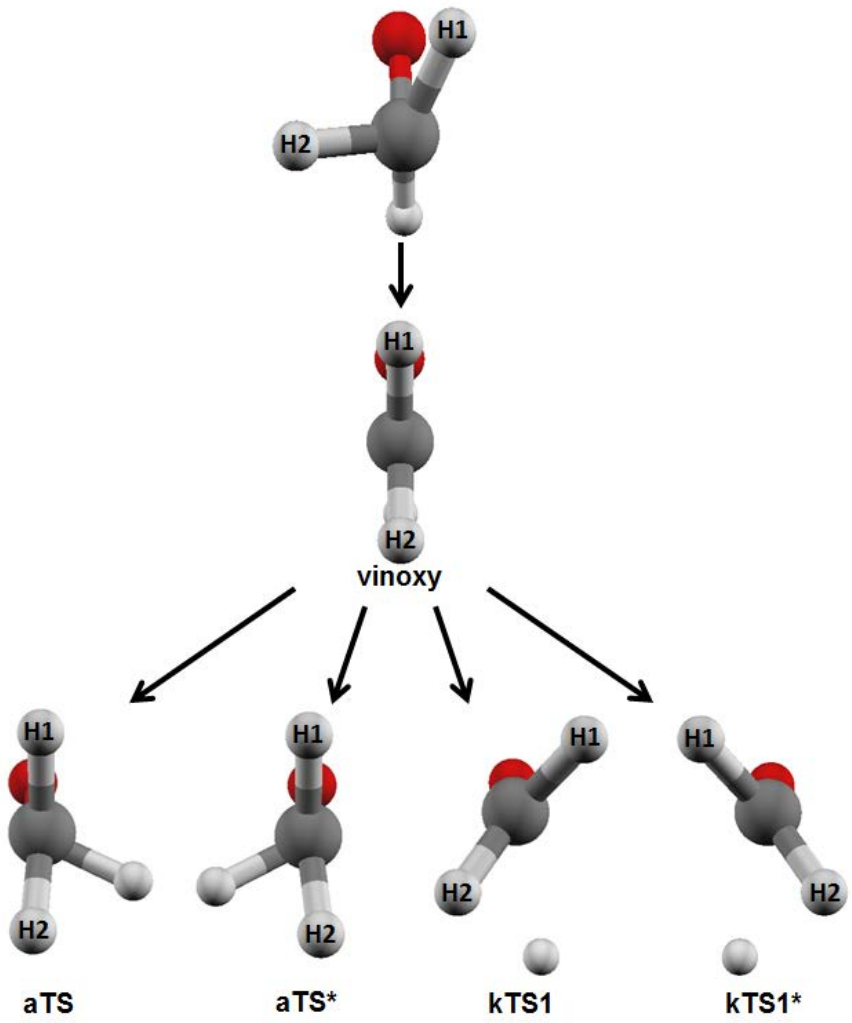

Figure S10. Permutations of the terminal H atoms used to get from the moiety of the **1a** conformer of chloroacetaldehyde to the vinoxy radial and then to the given transition states. All of the geometries are shown looking down the C-C bond with the O atom on the back carbon. “H1” and “H2” were used to denote where the terminal H atoms in the moiety are going in the given stationary points. The “*” in the name of the transition states denotes that it is the enantiomer of the given transition state as can be seen in the figure.

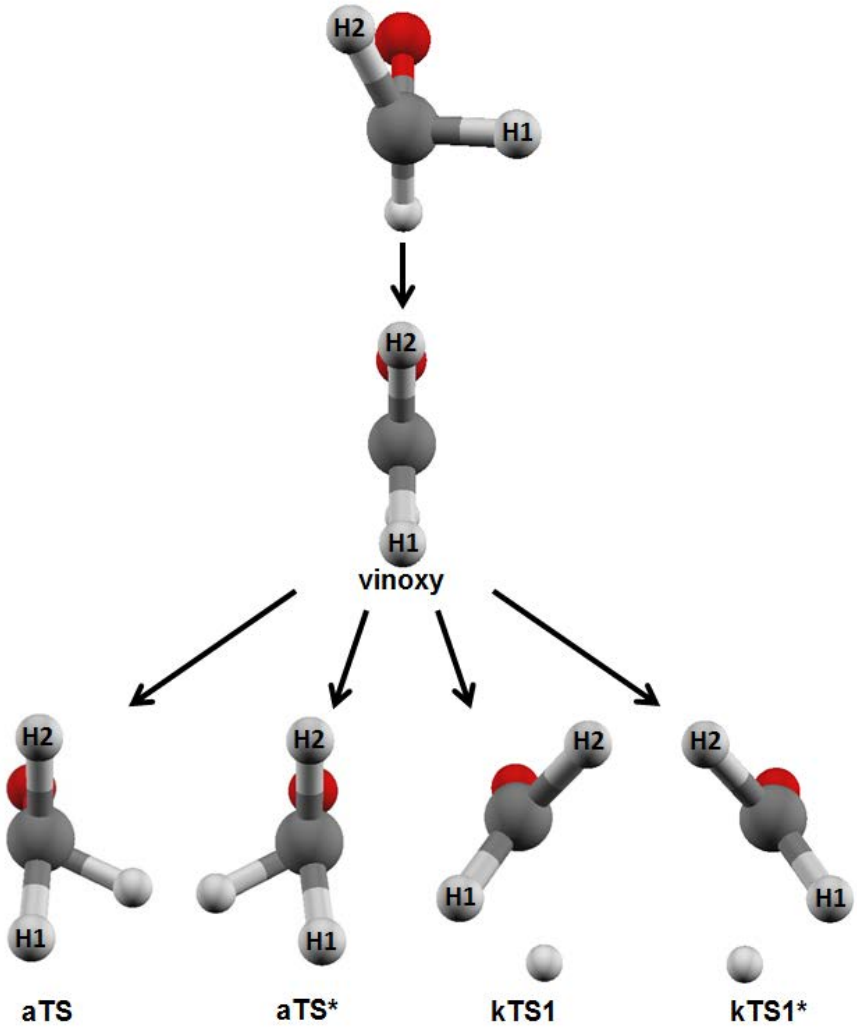

Figure S11. Permutations of the terminal H atoms used to get from the moiety of the **1b** conformer of chloroacetaldehyde to the vinoxy radical and then to the given transition states. All of the geometries are shown looking down the C-C bond with the O atom on the back carbon. “H1” and “H2” were used to denote where the terminal H atoms in the moiety are going in the given stationary points. The “*” in the name of the transition states denotes that it is the enantiomer of the given transition state as can be seen in the figure.

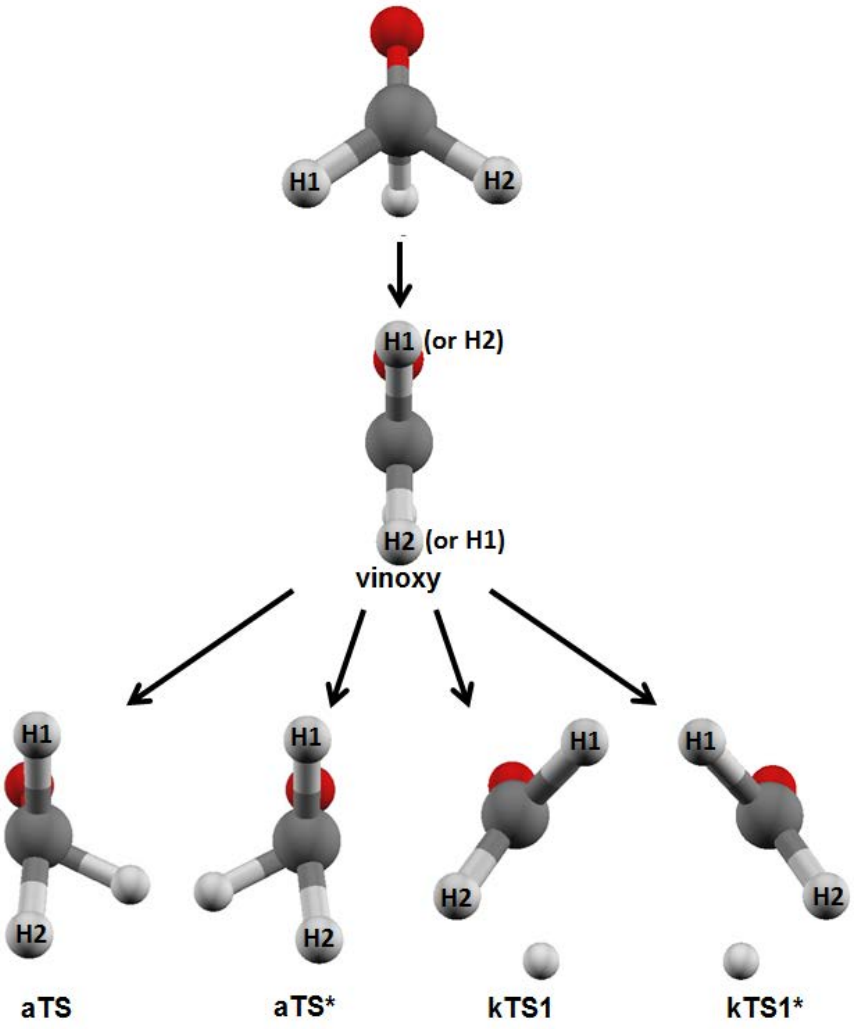

Figure S12. Permutations of the terminal H atoms used to get from the moiety of the **2** conformer of chloroacetaldehyde to the vinoxy radical and then to the given transition states. All of the geometries are shown looking down the C-C bond with the O atom on the back carbon. "H1" and "H2" were used to denote where the terminal H atoms in the moiety are going in the given stationary points. The "*" in the name of the transition states denotes that it is the enantiomer of the given transition state as can be seen in the figure. Note how due to the symmetry of this particular conformer the assignment of the terminal H atoms in the vinoxy radical can be done either way. Both assignments give the same rotational energies (i.e. E_{rot}/E_T), but the angular momentum vector has a different direction with respect to the geometry of the vinoxy radical.

G. E_T Dependence of the Branching Fraction for the H + ketene and methyl + CO channels

Anti conformer:

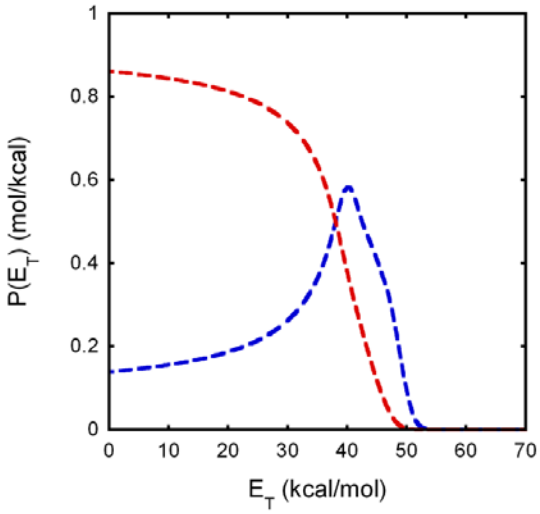

Figure S13. E_T dependence of the branching fraction for the H + ketene channel (shown in red) and the methyl + CO channel (shown in blue) from our branching calculations involving the anti conformer of chloroacetaldehyde. At higher E_T's the branching fractions do not sum to unity because some of the vinoxy radicals are stable.

Syn conformer:

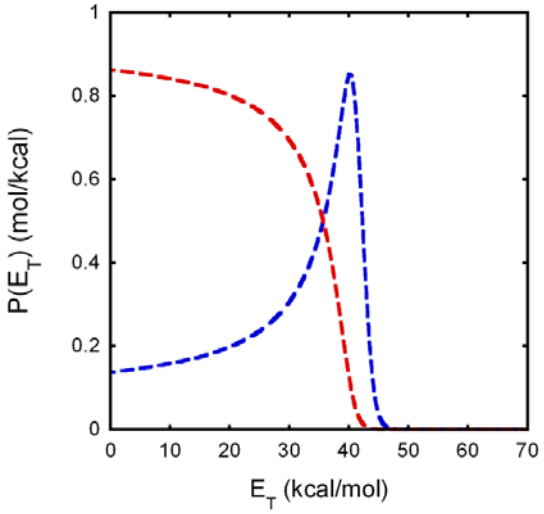

Figure S14. E_T dependence of the branching fraction for the H + ketene channel (shown in red) and the methyl + CO channel (shown in blue) from our branching calculations involving the syn conformer of chloroacetaldehyde.

H. Estimate of the $P(E_T)$ for a Minor HCl Elimination Channel

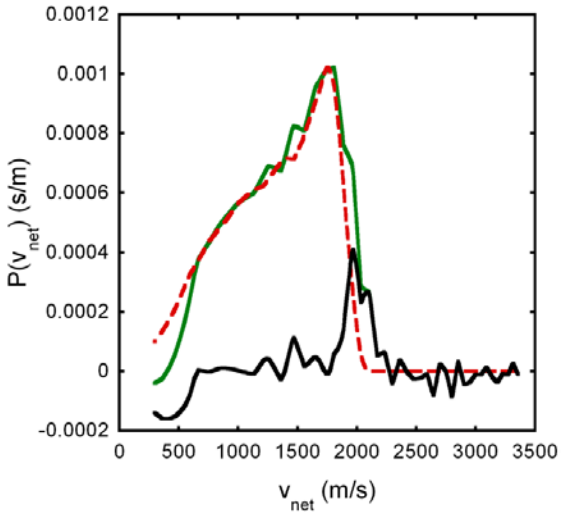

Figure S15. Experimental (solid green) and predicted (dashed red) speed distributions for ketene. The experimental speed distribution shown here came from the data in Figure 5, which was smoothed and interpolated. The predicted speed distribution was derived by converting the predicted portion of the C-Cl bond fission $P(E_T)$ that produces vinoxy radicals that dissociate to H + ketene from the branching calculations into a speed distribution with the appropriate Jacobian factors and assuming additional recoil velocity imparted to the ketene upon secondary dissociation is negligible. The black curve is the predicted speed distribution for the ketene that is unaccounted for, calculated from the difference between the green and red curves. It may be produced from primary HCl elimination of chloroacetaldehyde.

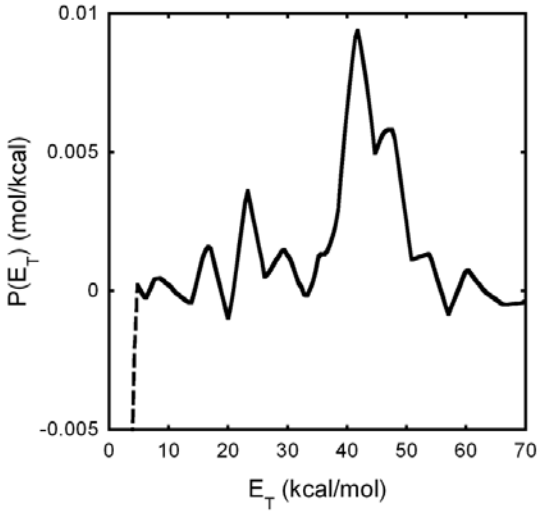

Figure S16. Predicted relative translational energy distribution, *$P(E_T)$*, for a possible primary HCl photoelimination channel from chloroacetaldehyde. The $P(E_T)$ shown is derived from the dashed black curve in Figure S15 by applying conservation of momentum, with m_1 = 42 (ketene) and $m_2 = m_{HCl}$, and Jacobian corrections. The dashed black portion of the *$P(E_T)$* represents where the values drop below zero due to possible decreased sensitivity close to the center of the phosphor screen.

I. Gaussian Convolution of the Predicted P(v_{net}) for the Methyl Signal from the Dissociative Ionization of Vinoxy to CH_3^+ + CO

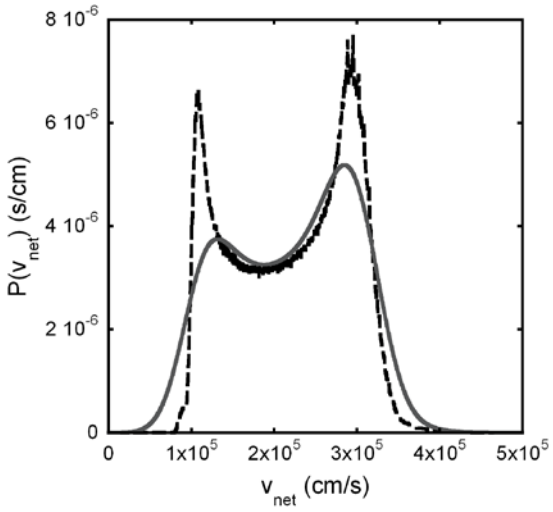

Figure S17. Gaussian convolution of the predicted P(v_{net}) for CH_3^+ from dissociative ionization of vinoxy. The dashed black line is the predicted P(v_{net}) of CH_3 yielded by dissociative photoionization of stable vinoxy radical, calculated from the $P(E_T)$ in gray from Figure 10 using the model described in Brynteson and Butler.[32] The solid gray line is the predicted P(v_{net}) convolved with a Gaussian function with a sigma of 25000 cm/s. We used this convolved P(v_{net}) in fitting the methyl signal shown in Figure 11.